

Inelastic collisions of ultra-cold heteronuclear molecules in an optical trap

Eric R. Hudson,* Nathan B. Gilfoy, S. Kotochigova,† Jeremy M. Sage,‡ and D. DeMille
Department of Physics, Yale University, 217 Prospect Street, New Haven, CT 06511, USA

Ultra-cold RbCs molecules in high-lying vibrational levels of the $a^3\Sigma^+$ ground electronic state are confined in an optical trap. Inelastic collision rates of these molecules with both Rb and Cs atoms are determined for individual vibrational levels, across an order of magnitude of binding energies. A simple model for the collision process is shown to accurately reproduce the observed scattering rates.

The electric dipole-dipole interaction provides a long-range, tunable anisotropic interaction between polar molecules. This is fundamentally different from most interactions studied between ultra-cold atoms, which are typically isotropic and comparatively short-ranged. Features of the dipole-dipole interaction can lead to many novel and exciting phenomena, such as field-linked states [1], long-range topological order [2], quantum chemistry [3, 4], and the possibility for quantum computation [5, 6]. Furthermore, the presence of closely spaced internal levels of the molecules, *e.g.* Ω -doublet, rotational, and vibrational levels, presents a host of new possibilities for precision measurement of fundamental physics [7, 8, 9, 10, 11]. Producing *ultra-cold* samples of polar molecules will facilitate trapping and, thus, the required high densities and long observation times for observing these phenomena.

Techniques such as Stark deceleration [12] and buffer gas cooling [13] are capable of producing cold samples from a wide range of molecular species; however, the temperatures and densities currently attainable via these “direct cooling” methods are not sufficient for observing many of the interesting phenomena mentioned above. Conversely, the association of ultra-cold atoms, either via a Feshbach [14] or optical resonance [15], restricts experiments to a limited class of molecules – namely, those composed of laser cooled atoms. Nonetheless, these methods are approaching temperatures and densities appropriate for observing the aforementioned phenomena.

In this Letter, we report the optical confinement of ultra-cold, vibrationally excited RbCs molecules in the $a^3\Sigma^+$ ground electronic state, produced via photo-association (PA) of laser-cooled ^{85}Rb and ^{133}Cs atoms. We utilize the long observation times afforded by the optical trap to determine the inelastic scattering rate for specific vibrational levels of these molecules, with both ^{85}Rb and ^{133}Cs atoms, across an order of magnitude of binding energies. We show that a simple model for the collision process accurately reproduces the observed scattering rates. We also extend this model to

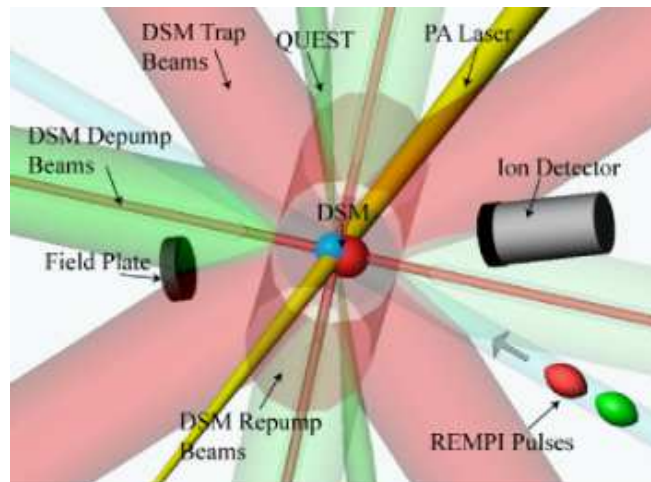


FIG. 1: (Color Online) Schematic of the experiment showing the overlap of the DSM with the relevant beams and relative position of the ion detector utilized in the state-selective REMPI detection.

estimate molecule-molecule inelastic scattering rates and discuss implications for producing trapped samples of $X^1\Sigma(v=0)$ RbCs molecules.

The apparatus used in this work is shown in Fig. 1. Briefly, ^{85}Rb and ^{133}Cs atoms are cooled and collected in a dual-species, forced dark-spot magneto-optical trap (DSM) [15, 16]. Using absorption imaging along two orthogonal directions we co-locate the species and measure the atomic density, n , and atom number, N , as $n_{\text{Rb}} = 4(2) \times 10^{11} \text{ cm}^{-3}$, $N_{\text{Rb}} = 9(1) \times 10^7$, and $n_{\text{Cs}} = 5(1) \times 10^{11} \text{ cm}^{-3}$, $N_{\text{Cs}} = 2(1) \times 10^8$. The temperature, T , of each species in the DSM was measured by time-of-flight expansion to be $T_{\text{Rb}} = (80 \pm 25) \mu\text{K}$ and $T_{\text{Cs}} = (105 \pm 40) \mu\text{K}$. Our optical trap is a quasi-electrostatic trap (QUEST) realized in a 1-D lattice configuration. The QUEST, represented by the green beam in Fig. 1, is formed by focusing and retro-reflecting the beam from a vertically-aligned 100 W CO_2 laser, operating with a 10.6 μm wavelength. An acousto-optical modulator placed in the beam path allows for the rapid turn-off of the QUEST ($\tau < 1 \mu\text{s}$) and serves as an optical isolator for light reflected back into the laser. The e^{-2} intensity beam waist at the focus is $\sim 75 \mu\text{m}$, yielding a peak intensity of $\sim 3 \text{ MW/cm}^2$ and trap depths of $\sim 4 \text{ mK}$, $\sim 6 \text{ mK}$, and $\geq 9 \text{ mK}$ for Rb, Cs, and $a^3\Sigma^+$ RbCs, respectively. Because

*Electronic address: Eric.Hudson@Yale.edu

†Department of Physics, Temple University, Philadelphia, Pennsylvania 19122-6082, USA

‡Lincoln Laboratory, Massachusetts Institute of Technology, Lexington, MA, 02420, USA

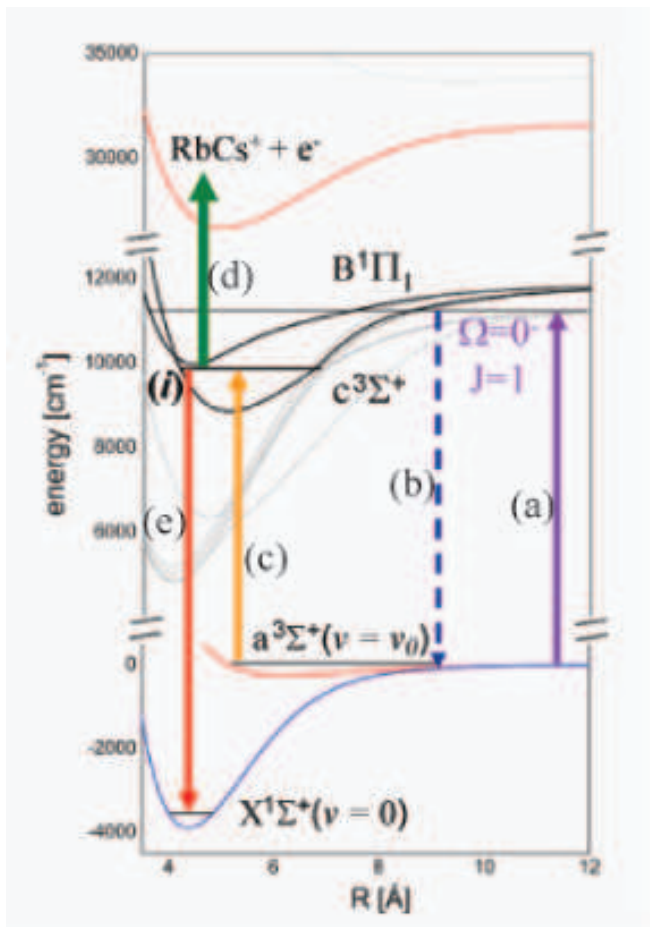


FIG. 2: (Color Online) Formation and detection processes for ultracold RbCs. (a) The PA process excites colliding atom pairs into bound RbCs* molecules, which (b) decay into a range of vibrational states of the $a^3\Sigma$ potential. (c) Metastable $a^3\Sigma(v)$ molecules are excited to level i , then (d) ionized and subsequently detected via time-of-flight mass spectrometry. The application of Stokes light (e) instead of the ionizing pulse (d) can be used to produce molecules in the absolute ground state $X^1\Sigma(v=0)$.

we utilize a lattice configuration for our QUEST, we are not restricted to trapping at the focus. We find it advantageous to trap atoms and molecules away from the focus, where the trap volume is much larger. By moving the point of overlap between the QUEST and DSM, we trap ~ 9 mm away from the focus, where the waist is ~ 400 μm and the trap depths are reduced by ~ 30 . In addition to providing a larger trapping volume, this method mitigates the effects of QUEST-induced light-shifts [17].

The energy level scheme relevant to the RbCs formation is shown in Fig. 2. The PA laser has an intensity of ~ 2 kW/cm^2 , and its frequency is locked to an $\Omega = 0^-$, $J_P = 1^+$ level, located 38.02 cm^{-1} below the Rb $5S_{1/2}(F=2) + \text{Cs } 6P_{1/2}(F=3)$ atomic asymptote [15]. Spontaneous decay of this state primarily produces molecules in the $a^3\Sigma^+$ state vibrational level with binding energy $E_B = -5.0 \pm 0.6$ cm^{-1} , to which we assign vibrational num-

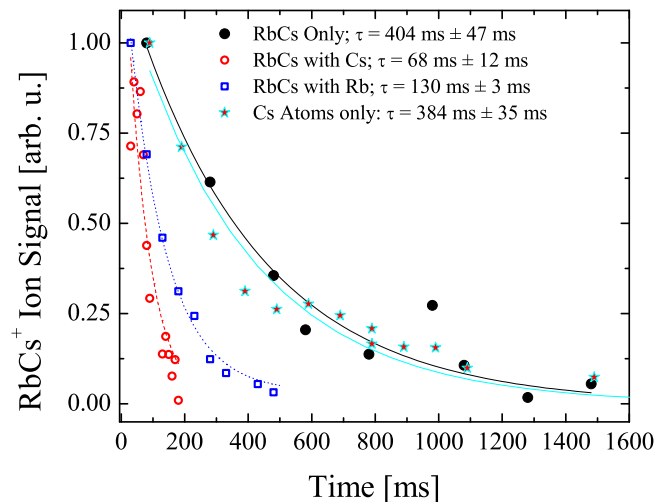


FIG. 3: (Color Online) Typical molecular lifetime data. Here the number of molecules in the $a^3\Sigma^+(v=v_0)$ state with binding energy $E_B = -5.0 \pm 0.6$ cm^{-1} is observed in the QUEST as a function of time. The presence of inelastic collisions between the atoms and molecules is evidenced by the dramatic reduction of the molecular lifetime when atoms are present. With no atoms we observe molecule lifetimes consistent with the background gas limited lifetime seen for isolated atomic clouds in the trap.

ber v_0 . In our previous work [18] we tentatively assigned $v_0 = 37$, but this value has an uncertainty of several units since the depth of the $a^3\Sigma^+$ state potential well is not accurately known.

Experimental data is taken by loading the DSM for 5 s from background alkali vapor, provided by heated getters, in the presence of both the PA laser and QUEST. Atoms are not efficiently loaded into the lattice directly from the DSM due to the low trap depth (~ 100 - 200 μK) away from the focus. Because the QUEST is substantially deeper for the molecules than the atoms (≥ 300 μK), the PA process efficiently loads RbCs into the lattice. Thus, molecules are loaded into the QUEST simply by applying the PA beam during the DSM loading process. From the measured atomic densities and known PA rates [18], we estimate that we trap $N_{\text{RbCs}} \approx 10^4$ molecules at a density of $n_{\text{RbCs}} \approx 10^9$ cm^{-3} and temperature of $T_{\text{RbCs}} \approx 100$ μK with roughly 7% in the $a^3\Sigma(v=v_0)$ state. To study atom-molecule collisions we load atoms into the lattice more efficiently via an optical molasses cooling stage for the desired atomic species, after the DSM is loaded. The optical molasses stage is performed by shifting the detunings, Δ , of the DSM trap lasers to $\Delta_{\text{Rb}} = -6\Gamma$, $\Delta_{\text{Cs}} = -16\Gamma$ for 10 ms, where Γ is the transition natural linewidth. While the hyperfine depumping beam of the DSM remains on during the entire molasses stage, the DSM hyperfine re-pumping beam is extinguished for the last 100 μs to ensure that all trapped atoms are in the lowest (dark) hyperfine state. Loading the lattice in this way leads to typical densities of $n_{\text{Rb}} = 2(1) \times 10^{11}$ cm^{-3}

and $n_{Cs} = 6(1) \times 10^{11} \text{ cm}^{-3}$, and temperatures of $T_{Rb} = (20 \pm 11) \text{ } \mu\text{K}$ and $T_{Cs} = (20 \pm 15) \text{ } \mu\text{K}$ in a volume of $\approx \pi(89 \text{ } \mu\text{m})^2 \times 960 \text{ } \mu\text{m}$, which is roughly a factor of 40 increase in density and factor of 5 reduction in temperature compared to loading directly from the DSM. After the molasses stage, we apply resonant ‘push’-beams for 10 ms to remove any undesired atoms from the lattice. After the ‘push’-beam sequence, all beams except the QUEST are shuttered, and the molecules and any deliberately trapped atoms are held in the lattice.

After a variable delay time, the QUEST is switched off and the trapped molecules are state-selectively ionized using Resonance-Enhanced Multi-Photon Ionization (REMPI), as shown in Fig. 1. The resulting ions are detected using time-of-flight mass spectrometry [19]. In this manner, we use the observed trap-lifetime of the molecules in the QUEST as a direct measurement of the molecular collision rates.

Typical lifetime data is shown in Fig. 3 for molecules in the $a^3\Sigma^+(v = v_0)$ state. As can be seen, the presence of atoms in the lattice significantly shortens the lifetime of the trapped molecules, which is otherwise limited by collisions with background gas. We attribute this behavior to inelastic collisions between the atoms and molecules. These losses are likely due to ro-vibrational quenching or hyperfine changing collisions. Each of these degrees of freedom carries sufficient energy that its relaxation creates enough kinetic energy to remove both the molecule and the atom from the trap, *e.g.* one vibrational quantum is $\sim 2 \text{ K}$. The number of trapped molecules, N_{RbCs} , evolves in time according to:

$$\frac{dN_{RbCs}}{dt} = -\Gamma_{BG}N_{RbCs} - \Gamma_{atom}N_{RbCs} - \frac{\beta}{V}N_{RbCs}^2. \quad (1)$$

Here Γ_{BG} is the loss rate due to collisions with background gas, Γ_{atom} is the loss rate due to inelastic collisions with atoms, β is the molecular 2-body loss rate, and V is the trap volume occupied by the molecules. Since two-body processes are negligible compared with background gas collisions ($\beta n_{RbCs}/\Gamma_{BG} \ll 1$), we use a fit of the data to the form of $N_{RbCs}(t) = N_0 e^{-t/\tau}$ with $\tau^{-1} = \Gamma_{atom} + \Gamma_{BG}$, to extract the value of Γ_{atom} . Γ_{atom} is related to the energy-dependent cross-section, $\sigma(E)$, and the relative velocity, v , as $\Gamma_{atom} = n_{atom} \langle \sigma(E)v \rangle$, where $\langle \rangle$ denotes thermal averaging. Hence, knowledge of the densities and temperatures allows the determination of the scattering rate constant, $K(T) = \langle \sigma(E)v \rangle$, for these collisions.

Because the initial PA process populates several vibrational states in the $a^3\Sigma^+$ state, we utilize the state-selectivity provided by the REMPI detection to measure data similar to that in Fig. 3 for a range of vibrational states and therefore, a range of binding energies, $E_B \approx -0.5 \text{ cm}^{-1}$ to -7 cm^{-1} . The results of the collision measurements are summarized in Fig. 4 as a function of E_B (measured relative to the $a^3\Sigma^+$ asymptote). The mea-

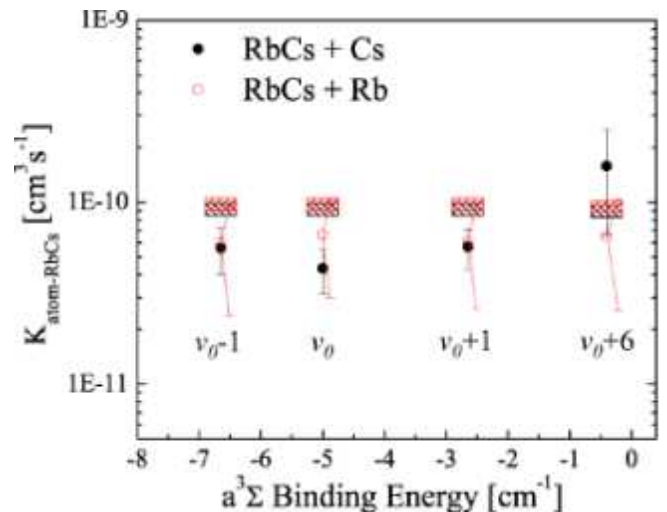


FIG. 4: (Color Online) . Molecular trap-loss scattering rate K constant vs. binding energy E_B , for molecules in specific vibrational levels of the $a^3\Sigma^+$ state. Vibrational state label appears below each data point. Despite more than an order of magnitude difference in binding energy, the scattering rates appear to be identical within experimental precision. The error bars on each point are the results of the uncertainties in the density and lifetime measurements. Note that the Rb data’s error bars have been angled for clarity. The black cross-hatched box and red hatched box are the prediction of the simple model described in the text for collisions with Cs and Rb, respectively. The width of the boxes is due to uncertainty in the collision temperature.

asured rate constants are identical within experimental precision, despite over an order of magnitude of variation in E_B . Since the molecule size and vibrational energy spacing both change substantially over this range of E_B , the lack of dependence of the scattering rate on molecular vibration hints at a unitarity limited process, where the details of the short-range interaction potential are unimportant. This view is supported by the agreement of the data with the results of a simple model of the collision process, shown in Fig. 4 as hatched boxes. This model [20], which is detailed below, simply assumes that any collision which penetrates to short-range results in an inelastic trap loss event. Thus, it represents a more accurate estimate of the upper-bound of an inelastic process than the usual Langevin (unitarity-limited) cross-section [21], which yields a scattering rate constant that is roughly two to three times larger [27].

For two colliding particles, the energy-dependent scattering cross-section for the ℓ th partial wave, with projection m , from state i to state f in all outgoing partial waves ℓ', m' is generally written as

$$\sigma_{\ell,m}(E, i \rightarrow f) = \frac{\pi}{k^2} \sum_{\ell', m'} |T_{\ell,m,\ell',m'}(E, i \rightarrow f)|^2. \quad (2)$$

Here $T_{\ell,m,\ell',m'}(E, i \rightarrow f)$ is the ‘T-matrix’, whose elements represent the probability amplitude for a transition from the incoming spherical wave, $\Psi_{i,\ell,m}$, to the

TABLE I: Calculated C_6 coefficients for $a^3\Sigma^+$ RbCs(v) colliding with various partners given in atomic units.

Collision Type	$(v_0 - 1)$	(v_0)	$(v_0 + 2)$	$(v_0 + 6)$
RbCs(v) + RbCs(v)	65745	65086	64310	61291
Rb + RbCs	16991	16920	16869	15960
Cs + RbCs	19688	19604	19541	18482

outgoing wave, $\Psi_{f,\ell,m'}$ and $k = \sqrt{2\mu E/\hbar^2}$ is the magnitude of the wave-vector at collision energy E . Since our experiments are sensitive to the total cross-section for collisions that remove molecules from the trap, we must sum over all final states f that lead to trap loss, in addition to the normal sum over ℓ, m . If we assume that any collision that penetrates to short-range is inelastic with unit probability, we can re-write Eq. (2) as

$$\sigma(E, i) = \sum_{f,\ell,m} \sigma_{\ell,m}(E, i \rightarrow f) = \sum_{\ell} \frac{\pi}{k^2} (2\ell + 1) P_T(E, \ell), \quad (3)$$

where $P_T(E, \ell)$ is simply the probability of transmission to short range. We calculate $P_T(E, \ell)$ by numerically solving the Schrödinger equation for the potential $V(r, \ell) = \frac{\hbar^2 \ell(\ell+1)}{2\mu r^2} - \frac{C_6}{r^6}$, and assuming that any flux that does not reflect off the potential is transmitted to short-range and then completely lost to inelastic processes. This simple technique is applicable to any highly-inelastic process; it requires only the knowledge of the long-range part of the scattering potential, which in our case is given entirely by the value of the van der Waals coefficient, C_6 , and reduced collision mass, μ .

In general, the C_6 constant for two colliding particles is given by the integral over imaginary frequency of the product of the particles' dynamic polarizabilities [22]. Since the dynamic polarizability of RbCs was calculated in Ref. [23] and the atomic values are well-known, the C_6 constant as a function of vibrational level is straightforward to calculate. These are shown for reference in Tab. I.

Using these values, P_T , σ , and K are calculated. The results are shown in Fig. 5, where the scattering rate, $K = \langle \sigma(E, i)v \rangle$, is plotted versus collision energy for the three classes of collisions. Note that the average center-of-mass frame collision velocity is given as $\langle v \rangle = \sqrt{\frac{8k_b T_1}{\pi m_1} + \frac{8k_b T_2}{\pi m_2}} = \sqrt{\frac{8k_b T_\mu}{\pi \mu}}$, where T_i (T_μ) is the laboratory frame (center-of-mass frame) temperature and m_i is the mass of the colliding particles. Since the $\ell = 1$ (p-wave) barrier heights lie at $E/k_B \approx 25$ μ K, 15 μ K, and 5 μ K for RbCs colliding with Rb, Cs, and RbCs, respectively, the collision rates fall to the values given solely by their s-wave contribution at the lowest energies on the graph. Interestingly, quantum reflection from the $\ell = 0$ potential is found to scale linearly with k as $E \rightarrow 0$, reproducing the Wigner threshold law [24] for low temperature inelastic scattering of $\sigma \propto 1/k$ [25]. Thus the calculated scattering rate remains finite at zero temperature, despite the fact that the unitarity limited scattering

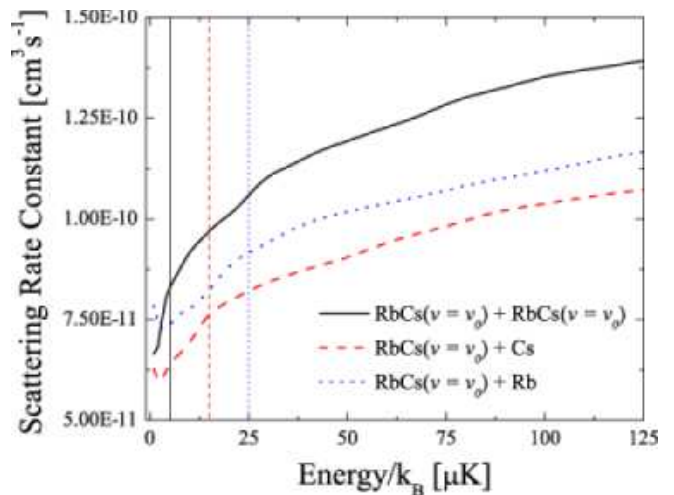


FIG. 5: (Color Online) Numerically calculated scattering rate constant vs. energy for the three types of collisions. The p-wave barrier height for each collision is represented by the vertical lines with the same plot-style (color).

rate scales as v^{-1} . From the predicted molecule-molecule scattering rate, we expect an initial two-body loss rate of $\frac{\beta}{V} N_{RbCs} = K n_{RbCs} \approx 0.1$ Hz. Given that $\Gamma_{BG} \approx 2$ Hz, our measurement of background gas limited decay for the pure RbCs sample is consistent with the predicted scattering rate.

In conclusion, we have demonstrated the trapping of heteronuclear RbCs molecules in vibrationally excited levels of the $a^3\Sigma^+$ electronic ground state. Observations of the molecules in the trap have revealed strong inelastic collisions, presumably due to a combination of vibrational, rotational and hyperfine quenching. A simple, extendable model, which relies only on the knowledge of the van der Waals coefficient, accurately reproduces the observed rates by assuming that all short-range collisions are inelastic for all observed vibrational levels and both colliding atomic species.

We are currently working towards transferring these trapped molecules into their absolute ground state, via the transfer scheme previously demonstrated in our lab [19]. It appears that with minimal improvements, *e.g.* implementing an adiabatic transfer [26] instead of the stimulated emission pumping used in [19], a sample of $> 10^4$ absolute ground state molecules $X^1\Sigma(v=0)$ at a temperature of 20 μ K and density of $\geq 10^9$ cm^{-3} can be created. From calculations of the adiabatic transfer with available laser powers, we estimate the transfer process can take place in ~ 100 μ s; thus, we anticipate negligible loss of population due to the inelastic collisions studied in the present work. In fact, it appears these inelastic collisions could serve a useful purpose. If Cs atoms are deliberately loaded into the lattice, any molecule not in the absolute ground state will quickly (~ 100 ms) be removed from the trap by these inelastic collisions. By contrast, $X^1\Sigma(v=0)$ molecules, which cannot undergo

inelastic collisions with Cs atoms, are unaffected by the presence of the atoms – even ground state molecules can have inelastic collisions with Rb atoms via the energetically allowed substitution reaction $\text{RbCs} + \text{Rb} \rightarrow \text{Rb}_2$

+ Cs. After the excited state molecules have been removed, resonant ‘push’-beams can eject the remaining atoms from the trap, leaving behind a pure sample of ground state molecules.

-
- [1] A. V. Avdeenkov, D. C. E. Bortolotti, and J. L. Bohn, *Phys. Rev. A* **69**, 012710 (2004).
- [2] A. Micheli, G. K. Brennen, and P. Zoller, *Nat. Phys.* **2**, 341 (2006), ISSN 1745-2473.
- [3] R. V. Krems, *Int. Rev. Phys. Chem.* **24**, 99 (2005).
- [4] E. R. Hudson et al., *Phys. Rev. A* **73**, 063404 (2006).
- [5] D. DeMille, *Phys. Rev. Lett.* **88**, 067901 (2002).
- [6] P. Rabl et al., *Phys. Rev. Lett.* **97**, 033003 (2006).
- [7] E. R. Hudson et al., *Phys. Rev. Lett.* **96**, 143004 (2006).
- [8] V. V. Flambaum and M. G. Kozlov, *Phys. Rev. Lett.* **99**, 150801 (2007).
- [9] D. DeMille et al., *Phys. Rev. Lett.* **100**, 023003 (2008).
- [10] D. DeMille et al., *Phys. Rev. Lett.* **100**, 043202 (2008).
- [11] T. Zelevinsky, S. Kotochigova, and J. Ye, *Phys. Rev. Lett.* **100**, 043201 (2008).
- [12] H. L. Bethlem, G. Berden, and G. Meijer, *Phys. Rev. Lett.* **83**, 1558 (1999).
- [13] J. M. Doyle et al., *Phys. Rev. A* **52**, R2515 (1995).
- [14] S. Inouye et al., *Phys. Rev. Lett.* **93**, 183201 (2004).
- [15] A. Kerman et al., *Phys. Rev. Lett.* **92**, 033004 (2004).
- [16] M. H. Anderson et al., *Phys. Rev. A* **50**, R3597 (1994).
- [17] P. F. Griffin et al., *New J. of Phys.* **8**, 11 (2006), ISSN 1367-2630.
- [18] A. Kerman et al., *Phys. Rev. Lett.* **92**, 153001 (2004).
- [19] J. M. Sage et al., *Phys. Rev. Lett.* **94**, 203001 (2005).
- [20] C. Orzel et al., *Phys. Rev. A* **59**, 1926 (1999).
- [21] P. S. Julienne and J. Vigue, *Phys. Rev. A* **44**, 4464 (1991).
- [22] A. Derevianko et al., *Phys. Rev. Lett.* **82**, 3589 (1999).
- [23] S. Kotochigova and E. Tiesinga, *Phys. Rev. A* **73**, 041405 (2006).
- [24] E. P. Wigner, *Phys. Rev.* **73**, 1002 (1948).
- [25] N. Balakrishnan, R. Forrey, and A. Dalgarno, *Chem. Phys. Lett.* p. 1 (1997).
- [26] K. Bergmann, H. Theuer, and B. W. Shore, *Rev. Mod. Phys.* **70**, 1003 (1998).
- [27] The Langevin scattering rate is given as $K_{Langevin} = \left\langle \frac{v\pi}{k^2} \sum_{\ell}^{\ell^{max}} (2\ell + 1) \right\rangle = \left\langle \frac{\hbar\pi}{\mu k} (\ell^{max} + 1)^2 \right\rangle$, where ℓ^{max} is defined as the value of ℓ for which the centrifugal barrier of the collision potential equals the kinetic energy of the colliding particles.